



Molecular Crystals and Liquid Crystals

Publication details, including instructions for authors and subscription information:

<http://www.tandfonline.com/loi/gmcl20>

Optical Properties of Cholesteric Materials used in Surface Stabilised Cholesteric Texture Devices

N. W. Roberts^a, J.-P. S. Guillou^a, H. F. Gleeson^a,
I. Kirar^a, S. J. Watson^a & E.O. Arikainen^a

^a Department of Physics and Astronomy, University of Manchester, UK

Published online: 18 Oct 2010.

To cite this article: N. W. Roberts, J.-P. S. Guillou, H. F. Gleeson, I. Kirar, S. J. Watson & E.O. Arikainen (2004) Optical Properties of Cholesteric Materials used in Surface Stabilised Cholesteric Texture Devices, *Molecular Crystals and Liquid Crystals*, 411:1, 57-70, DOI: [10.1080/15421400490434793](https://doi.org/10.1080/15421400490434793)

To link to this article: <http://dx.doi.org/10.1080/15421400490434793>

PLEASE SCROLL DOWN FOR ARTICLE

Taylor & Francis makes every effort to ensure the accuracy of all the information (the "Content") contained in the publications on our platform. However, Taylor & Francis, our agents, and our licensors make no representations or warranties whatsoever as to the accuracy, completeness, or suitability for any purpose of the Content. Any opinions and views expressed in this publication are the opinions and views of the authors, and are not the views of or endorsed by Taylor & Francis. The accuracy of the Content should not be relied upon and should be independently verified with primary sources of information. Taylor and Francis shall not be liable for any losses, actions, claims, proceedings, demands, costs, expenses, damages, and other liabilities whatsoever or howsoever caused arising directly or

indirectly in connection with, in relation to or arising out of the use of the Content.

This article may be used for research, teaching, and private study purposes. Any substantial or systematic reproduction, redistribution, reselling, loan, sub-licensing, systematic supply, or distribution in any form to anyone is expressly forbidden. Terms & Conditions of access and use can be found at <http://www.tandfonline.com/page/terms-and-conditions>

OPTICAL PROPERTIES OF CHOLESTERIC MATERIALS USED IN SURFACE STABILISED CHOLESTERIC TEXTURE DEVICES

N. W. Roberts, J.-P. S. Guillou, H. F. Gleeson, I. Kirar,
S. J. Watson, and E. O. Arikainen
Department of Physics and Astronomy, University
of Manchester, M13 9PL, UK

An in depth study has been made of the optical properties of a series of non-thermochromic chiral nematic materials to determine the influence of refractive index dispersion on pitch measurements. The materials used were mixtures of a chiral nematic material, BL131a, and a nematic material BL130 (from Merck Ltd.) in which the pitch is changed by varying the concentration of the nematic component. Detailed measurements were made of the ordinary and extraordinary refractive indices as a function of wavelength across the visible spectrum. Dispersion effects changed the birefringence by approximately 10% across the visible spectrum. Reflection spectra were obtained and used to deduce the helicoidal pitch. Failure to include dispersion in the calculation led to a significant error in calculations of both the bandwidth and pitch of the material. Finally, as SSCT devices are electro-optic in nature, the influence of the conducting surface of the device on the optical properties is examined.

INTRODUCTION

One of the best known optical phenomena in liquid crystals is the selective reflection of light from cholesteric (chiral nematic) materials which is responsible for the bright, iridescent colours observed in a planar sample. Of course, not all chiral nematic textures reflect or scatter light strongly and the focal conic texture in particular scatters light rather weakly. In the focal conic texture, the direction of the optic axis is no longer exclusively perpendicular to the substrate, instead there are many domains each

This work has been funded by EPSRC grant number GR/M/70858 and the British Council (IK) under the international exchange student scheme. The authors would like to thank Merck for supplying the materials used in this investigation.

Address correspondence to H. F. Gleeson, Department of Physics and Astronomy, University of Manchester, M13 9PL, United Kingdom.

with its own optic axis direction. Application of an electric field can cause switching between the planar and focal conic textures, either directly or via the relaxation of other textures. Moreover, with the creation of permanent domains within the structure, each texture (planar and focal conic) becomes stable [1] forming the basis for the so-called surface-stabilised cholesteric texture (SSCT) device. Suitable domains can be achieved either through the polymerisation of a monomer dispersed throughout the liquid crystal [2] or by using surface alignment [3] and the advantages of each method of device production have been compared elsewhere [4].

SSCT devices are particularly attractive because of their low power consumption, a result of the bistability of the two textures and the fact that the display is reflective so no back-light is needed. The displays can take many slightly different forms and the technology is now commercially available [5], making it important that materials designed for use in such devices are fully characterised. This paper reports the optical properties of a family of mixtures designed for use in SSCT displays, indicating how dispersion in the refractive index influences calculation of the pitch from selective reflection spectra and how confinement of the material within a device changes its optical characteristics. The materials studied are not thermochromic and the pitch of individual mixtures is varied by the addition of the nematic material BL130 to the chiral nematic material BL131a, a system designed by Merck Ltd [6]. This type of material provides a whole palette of colours and, at the same time, satisfies the requirements for the thermal operational stability in a display. The elastic constants and viscosity of this family of materials are reported elsewhere [7].

THEORETICAL BACKGROUND

The optical properties of the planar chiral nematic texture are well known and at normal incidence simple equations describe the central wavelength, λ_o , and the band width, $\Delta\lambda$, of the reflection band;

$$\lambda_o = \bar{n}p \quad \text{and} \quad \Delta\lambda = \Delta np. \quad (1)$$

In Eq. (1), \bar{n} is the mean refractive index $((n_o + n_e)/2)$, Δn is the birefringence and p is the helicoidal pitch of the chiral nematic material. Ferguson [8] further deduced an equation that approximately describes the wavelength for non-normal incidence or for polydomain samples;

$$\lambda = \frac{p\bar{n}}{m} \cos \left[\frac{1}{2} \sin^{-1} \left[\frac{\sin \theta_i}{\bar{n}} \right] + \frac{1}{2} \sin^{-1} \left[\frac{\sin \theta_r}{\bar{n}} \right] \right], \quad (2)$$

where θ_i and θ_r are the angle of incidence and reflection respectively and m is an integer (usually 1). While Eq. (2) is useful in making small

corrections to the observed wavelength for a sample illuminated with obliquely incident light, it is only valid for small angles. However, the dielectric tensor for a chiral nematic material is well-known and the reflection spectrum of a planar sample can be calculated from the solution of Maxwell's equations for light propagating within the medium. This is most easily done numerically using the Berreman technique [9], the approach employed in this work when exact comparisons were necessary between the reflection spectra and the parameters for the cholesteric thin films under investigation.

Both Eqs. (1) and (2) assume that the refractive index is a constant with respect to wavelength, a factor that has long been known to produce discrepancies between measured and predicted values of the pitch and reflection band width [10]. Molecular polarisabilities are frequency dependent, so refractive indices are subject to dispersion, as can be described by Sellmeier's equation [11],

$$n^2 = 1 + \frac{B\lambda^2}{\lambda^2 - \lambda_1^2}, \quad (3)$$

where λ is the wavelength at which the refractive index n is measured and B and λ_1 are fitting parameters. The extent to which the phenomenon of dispersion must be taken into account in the prediction of optical properties from measured quantities will clearly depend on the system under consideration. This paper presents the refractive indices of a family of mixtures of chiral nematic liquid crystals measured as a function of wavelength and uses the data to deduce the pitch of the materials from the reflection spectra.

EXPERIMENTAL

The materials employed were mixtures of a two-component system designed by Merck for use in SSCT devices, a nematic host, (BL130), and a chiral mixture (BL131a) selected such that the reflection band is centred at a low wavelength in the visible spectrum (tight pitch). Dilution of the pitch of BL131a with BL130 allows the reflection band to be shifted through the visible spectrum to longer wavelengths. Temperature was maintained at $25 \pm 0.1^\circ\text{C}$ for all measurements presented in this paper.

The refractive indices of the liquid crystal mixtures were measured using an Abbé 60 refractometer from Bellingham and Stanley Ltd. Information regarding the dispersion of the prism was supplied with the refractometer and was taken into account when deducing the values of liquid crystal refractive index. The inherent accuracy of the Abbé refractometer used was 10^{-4} .

The optic axis of a cholesteric liquid crystal coincides with the helical axis so the birefringence is strictly negative. It is most convenient to measure the refractive indices of a cholesteric sample using a planar geometry (the helicoidal axis is perpendicular to the faces of the prisms) which gives optimum alignment, in contrast to the homeotropic alignment usually used for nematic samples. Planar alignment is readily achieved by wiping the surfaces of the refractometer prisms with a dilute solution of polyvinyl alcohol. In common with measurements on nematic samples, the ordinary and extraordinary refractive indices can be distinguished through their polarisation. In the planar geometry, the measured ordinary refractive index of the helicoidal cholesteric structure is an average of the refractive indices parallel and perpendicular to the director (perpendicular to the helicoidal axis) [12,13]. For the sake of clarity the *measured* refractive indices for the cases of cholesteric and nematic liquid crystals are summarised in Table 1. While there is clear correspondence between the lowest refractive indices measured on the refractometer and the values perpendicular to the director (n_{\perp}) for both nematic and cholesteric samples, the highest value corresponds to the parallel value (n_{\parallel}) only for the nematic case. For cholesteric samples, the high value of refractive index measured ($n_{o,Ch}^*$) is an average of the two refractive indices and n_{\parallel} must be deduced according to the equation given in Table 1.

The dispersion in refractive index was determined by making measurements at wavelengths across the visible spectrum. A microscope lamp was used as a broad band light source and specific wavelengths were selected using a monochromator. The experimental errors of the measurements varied slightly with the wavelength, increasing closer to the extremes of the visible spectrum where the sensitivity of the observer's eye reduces. In this work, each data point is the mean of ten measurements and the standard deviation of these measurements (which normally exceeds the nominal accuracy of the refractometer) is used to define the uncertainties in refractive index measurements.

TABLE 1 A Summary of the Relationship Between the Measured Refractive Indices for a Homeotropic Nematic Sample (Subscripts 'N') and a Planar Chiral Nematic Sample (Subscripts 'Ch') Using an Abbé Refractometer. The Parameters n_{\perp} and n_{\parallel} are the Refractive Indices Perpendicular to and Parallel to the Local Director Respectively

	Measured low refractive index	Measured high refractive index
Nematic	$n_{o,N} = n_{\perp}$	$n_{e,N} = n_{\parallel}$
Chiral nematic	$n_{e,Ch} = n_{\perp}$	$n_{o,Ch}^* = \sqrt{\frac{1}{2}(n_{\perp}^2 + n_{\parallel}^2)}$

Figure 1 shows a diagram of the experimental layout used to obtain selective reflection spectra. Planar devices of nominal thickness $5\text{ }\mu\text{m}$ were placed under a polarising reflection microscope and illuminated using a $10\times$ objective lens. The cone of illumination of the sample and the collection of reflected light has a maximum angle defined by the numerical aperture (N.A = 0.22) of the objective lens used. The influence of oblique incidence caused by different numerical apertures was investigated and the errors introduced by the lens used were found to be insignificant [14]. The light output from the second reflection arm of the microscope was directed into a monochromator, dispersed by a diffraction grating (1200 lines/cm) and ultimately detected by a photo-multiplier tube (PMT) connected to an amplifier. The voltage output was measured by a digital voltmeter connected to a personal computer that also controlled the monochromator.

In most cases, the reflection spectra are presented without having been normalised for the chromatic response of the system (resulting from a combination of the response of the PMT and the white light spectrum of the illuminating bulb). Where some comparison of intensity across the wavelength scale was required, the spectra were normalised for the shape of the chromatic response. In general, because the intensity of incident light and other parameters of importance were adjusted to optimise each spectrum, the values of the intensity from one spectrum to another should not be compared directly.

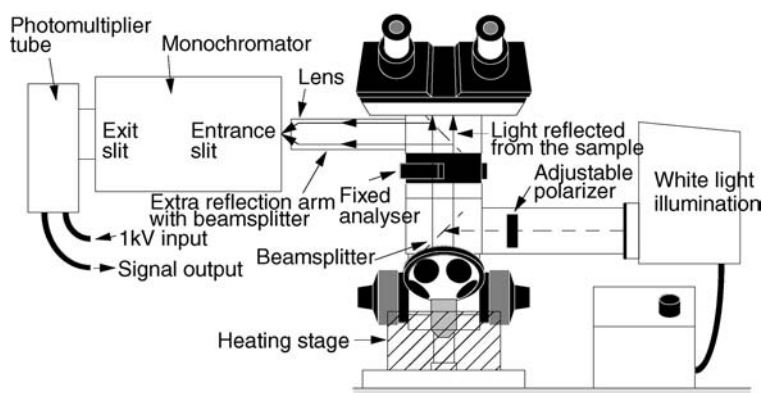


FIGURE 1 Apparatus to measure the selective reflection spectra of cholesteric films.

RESULTS AND DISCUSSION

1. Refractive Index Measurements

The form of the refractive index variation of the materials as a function of incident wavelength was similar at all concentrations. A typical dispersion curve for the refractive indices $n_{\parallel}(\lambda)$ and $n_{\perp}(\lambda)$ and the calculated average refractive index $\bar{n}\lambda$ is shown in Figure 2 for the 100% chiral material, BL131a. All the refractive indices decrease with increasing wavelength, as expected. In all of the mixtures studied, the absolute refractive index changes across the visible range (from 480 to 630 nm) are relatively small: 0.03 for n_{\parallel} , 0.01 for n_{\perp} and 0.025 for \bar{n} . Figure 3 illustrates the effect of dispersion on the birefringence for three different mixtures. It can be seen that whilst the absolute change in Δn is rather small, the relative value decreases by around 10% on changing the illumination wavelength from 480 nm to 650 nm.

2. Selective Reflection Measurements

It is possible to determine the helicoidal pitch of a cholesteric material from several points on the reflection spectrum of a planar sample, the most obvious choices being the centre and two extremes of the reflection band.

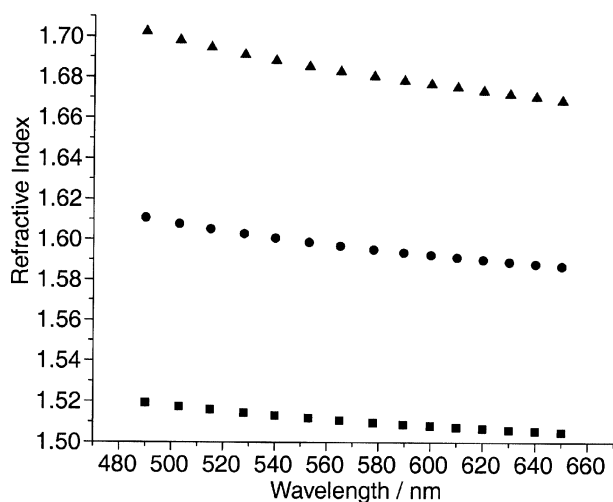


FIGURE 2 The dispersion data for all the refractive indices of the 100% cholesteric mixture BL131a. The triangles correspond to n_{\parallel} , squares to n_{\perp} and circles to \bar{n} .

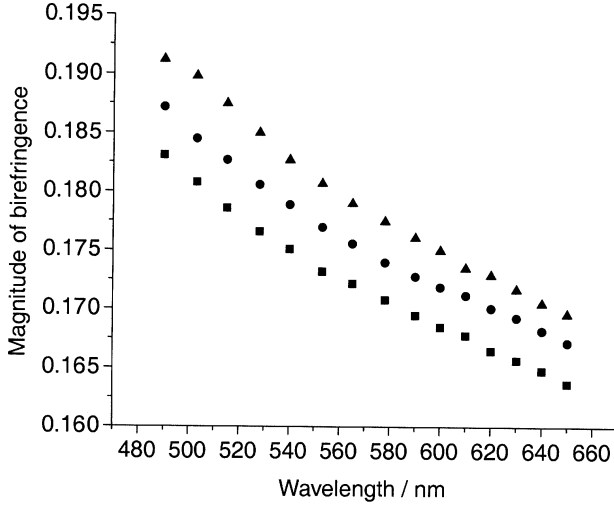


FIGURE 3 The wavelength dependence of the magnitude of the birefringence $\Delta n(\lambda)$ in three different mixtures of BL131a/BL130. The squares, circles and triangles correspond to 100%, 75% and 50% of BL131a respectively. Note that the sign of the birefringence for the nematic material is strictly positive, while the cholesteric mixtures all have negative birefringence because of their structure.

If these wavelength values are defined as λ_0 , λ_1 and λ_2 respectively, with $\lambda_1 < \lambda_2$, the pitch is given equivalently by:

$$p = \frac{\lambda_0}{\bar{n}} = \frac{\lambda_1}{n_{\perp}} = \frac{\lambda_2}{n_{\parallel}}, \quad (4)$$

The wavelengths of the theoretical points ($\lambda_0, \lambda_1, \lambda_2$) were calculated from defined points on experimental spectra as shown in Figure 4,

$$\lambda_0 = \frac{\lambda_1 + \lambda_2}{2}, \quad \lambda_1 = \frac{\lambda_{1(low)} + \lambda_{1(high)}}{2}, \quad \lambda_2 = \frac{\lambda_{2(low)} + \lambda_{2(high)}}{2}, \quad (5)$$

The error in assigning the points $\lambda_{1(low)}$, $\lambda_{1(high)}$, $\lambda_{2(low)}$ and $\lambda_{2(high)}$ defined in the figure was better than ± 0.5 nm, by far the dominant error in the measurement. However, if the pitch is calculated using Eq. (4) and the refractive indices are measured at a single wavelength (usually $\lambda = 589.6$ nm) [10], poor agreement in the pitch values is often obtained. Indeed, strictly Eq. (4) should have been written:

$$p = \frac{\lambda_0}{\bar{n}(\lambda_0)} = \frac{\lambda_1}{n_{\perp}(\lambda_1)} = \frac{\lambda_2}{n_{\parallel}(\lambda_2)}, \quad (6)$$

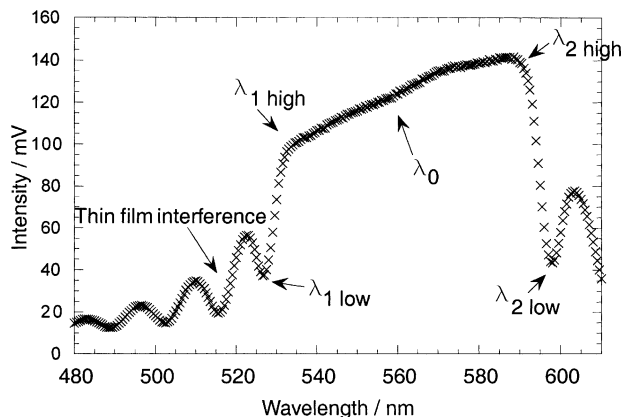


FIGURE 4 An example of the selective reflection spectrum showing the thin film interference and the positions taken for $\lambda_{1(\text{low})}$, $\lambda_{1(\text{high})}$, λ_0 , $\lambda_{2(\text{low})}$, $\lambda_{2(\text{high})}$.

where $\bar{n}(\lambda_0)$ should be read 'the average refractive index at a wavelength of λ_0 '.

Figure 5 illustrates this point. The bar graph shows the difference between measured pitch values at concentrations of 75%, 85%, 95% and 100%, calculated using Eq. (5), both with and without the dispersion taken into account. In the calculation without the dispersion, the refractive indices were measured at a wavelength of 589.6 nm. The bar graph clearly shows that the error in the pitch measurement becomes greater the further

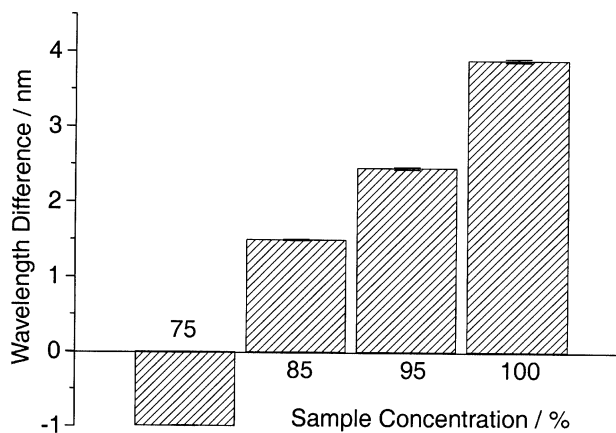


FIGURE 5 The difference between pitch measurements taking into account the dispersion relation and using refractive indices measured at 589.6 nm.

the reflection peak moves away from the single wavelength used in the refractive index measurement. However, Figure 5 also shows that while dispersion must be taken into account to obtain accurate measurements of the pitch from any part of the reflection spectrum, the effect is rather small. It is perhaps also worth noting that the error will be enhanced for cholesteric materials that absorb, such as some of the recently reported polymeric systems [15]. Then the dispersion becomes significant close to an absorption edge so that the bandwidth will relate rather poorly to the birefringence measured at a single wavelength.

3. Influence of the Indium Tin Oxide (ITO)

The two stable states in an SSCT device are voltage-selected so devices must be constructed with transparent electrodes. Reflections at conducting and dielectric interfaces differ in that the former always produce a phase change, a phenomenon that might be expected to change the optics of a reflection from chiral nematic films. Indeed, such an observation is readily made; examination of the electrode area using linearly polarised light is qualitatively different from the appearance of the non-electrode area under identical viewing conditions as shown in Figure 6. As SSCT devices are not designed for use with polarisers, this observation seems at first to be of little interest. However, the method proposed to obtain full colour from such devices is to stack layers with overlapping reflection bands. As the light transmitted through a planar slab of cholesteric material within the reflection band has rather specific polarisation states at different wavelengths, the optical properties of the combined device in the overlap regions can certainly be influenced. The following section considers the polarisation dependence of the reflection band of a cholesteric sample

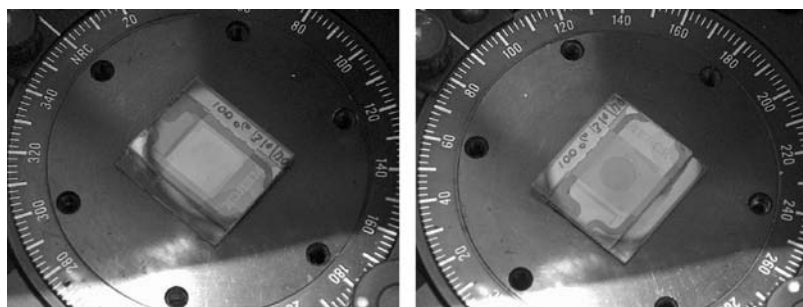


FIGURE 6 Two photographs showing the change in appearance after a 90° rotation of the planar state of an SSCT device viewed using linear polarised light. The electrode area is in the central region of the device.

using plane polarised light – approximately the polarisation state expected at the edges of the reflection band where the overlap region of two different layers is most likely to lie.

Consider the measured spectra shown in Figure 7, which are typical of the reflection spectra obtained for polarised light both a) off and b) on the ITO area. In both cases it is clear that outside the reflection band the finite thickness of sample results in distinct interference fringes, however within the reflection band, fringes can only be seen from the ITO area of the cell. It is interesting to consider simplistically the differences between the two cases. Ray 1 in Figure 8 corresponds to light at normal incidence and at a wavelength within the reflection band of a cholesteric liquid crystal held between glass substrates; its polarisation state is in general elliptical with a handedness that depends on the material and position within the reflection band. Ray 2 is ‘reflected’ with the opposite sense of elliptical polarisation to that of the helix because of the periodic nature of the liquid crystal. The remainder of the light, ray 3, must therefore be elliptically polarised with the same sense as the helix as it propagates through the cell and emerges as ray 4. For interference to occur in the space beyond the upper substrate of the cell, some percentage of ray 3 must be reflected at the bottom interfaces and be of the allowed elliptical polarisation such that it can propagate back through the helix. The reflection is due to the dielectric boundaries between the liquid crystal, alignment layer, glass and air. In the case without the ITO layer, the reflection takes place at several interfaces; both dense to rare ($\bar{n}_{\text{(liquid crystal)}} \approx 1.6/\bar{n}_{\text{(glass)}} \approx 1.5$ and $\bar{n}_{\text{(glass)}} \approx 1.5/\bar{n}_{\text{(air)}} \approx 1.0$) and rare to dense ($\bar{n}_{\text{(alignment layer)}} \approx 1.45/\bar{n}_{\text{(glass)}} \approx 1.5$). Upon both the dense to rare reflections there is a π phase change. This reverses the sense of

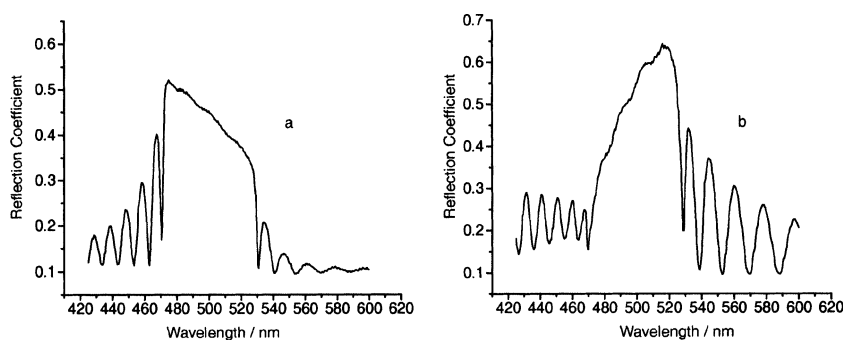


FIGURE 7 Example of a reflective spectrum taken a) off and b) on the area of the ITO electrodes. In b) note the thin film interference fringes seen within the reflection band. In both plots the incident linear polarisation is perpendicular to the surface alignment.

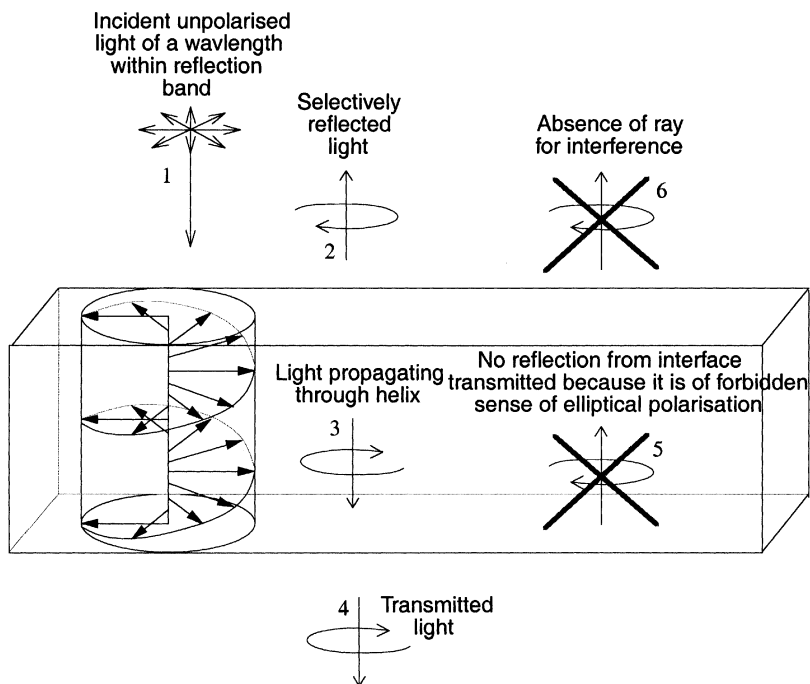


FIGURE 8 A diagram showing the allowed polarisations of light of a wavelength within the reflection band incident on a cell without the conducting ITO layer.

polarisation, no longer matching the handedness of the ray and the helix, and thus not allowing ray 5 to propagate back through the liquid crystal. Also there is the rare to dense reflection, however, although the reflected ray can now propagate back though, the refractive index difference between the media is not great enough to provide an appreciable intensity to cause easily observable interference fringes. Therefore, without the ITO layer, no interference is observed within the reflection band. However, with the ITO present, ray 3 is also reflected from a rare to dense interface at the metal ITO boundary. This also causes a phase change upon reflection but in general it does not equal π [16], thus providing a component of the reflected ray that matches the handedness of the helix. Hence ray 5 is now allowed to propagate back through the liquid crystal, causing the interference fringes within the reflection band. Although this is a somewhat simplistic explanation, from experimental evidence it does explain the features of the reflection spectra measured on and off the ITO area of the cell. It is also worth noting, that the slope of the spectrum differs between a) and b) in Figure 7. The wavelength

of the maximum value of the reflection coefficient clearly explains the colour differences seen between the ITO and outside area in Figure 6.

To investigate the reflection spectra from the ITO areas further, polarisation-dependent reflection spectra of a planar aligned cell were taken for incident polarisation directions at intervals of 30° with respect to the rubbing direction of the alignment layer and normalised for the chromatic response of the apparatus, (Fig. 9(a) and (c)). These experimental reflection spectra are compared to numerical reflection spectra (Fig. 9b and (d)) calculated using the Berreman 4×4 method. Included in these calculations are the glass/ITO/alignment layers and it is clear that the complex refractive indices of the ITO layer predict the thin film inter-

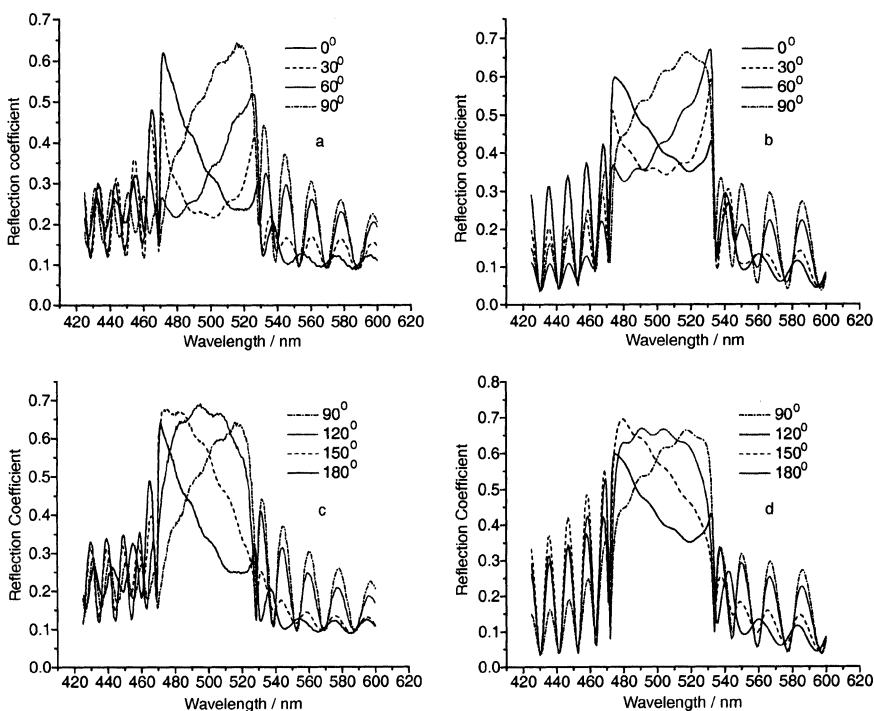


FIGURE 9 Normalised reflection spectra as a function of changing angle of input linear polarisation a) experimental reflection spectrum from a rotation of the cell from 0° to 90° polarisation and b) theoretical reflection spectrum from a rotation of the cell from 0° to 90° and c) reflection spectra from a rotation of the cell from 105° to 180° shown with constant input polarisation and no analyser and d) theoretical reflection spectrum from a rotation of the cell from 90° to 180° .

ference seen within the reflection band. The quality of agreement also demonstrates the accuracy of both the model and the experimental data.

CONCLUSIONS

The investigation presented here has demonstrated that care must be taken when calculating the pitch from reflection spectra. Without consideration of the dispersion of the refractive indices and an awareness of the preferred pitch in aligned cells it is possible that the specification of these materials' properties with a view to their display application could be misleading. Beyond these static display properties, the dynamic properties of the materials such as response and relaxation time will be considered in a future publication. The investigation has also analysed the contrasting optics between reflections from the ITO area of the cell and that outside of the electrode area. Agreement between experimental measurements and theoretical modelling clearly showed the interference fringes seen within the reflection band are simply explained with the correct consideration of optical multi-layer effects due to the cell's construction. With this complete characterisation of the display device parameters, it should be possible for these materials, or those developed from them, to be widely used in the display market.

REFERENCES

- [1] Lu, M. (1997). *J. Appl. Phys.*, 81, 1063.
- [2] Chien, L. C., Nabor, M. F., & Muller, U. (1995). *Abstracts of Papers of the American Chemical Society*, 209, 274.
- [3] Chang, C. (1999). Asia Society for Information Display Conference Proc., 227.
- [4] Yang, D. K., West, J. L., Chein, L. C., & Doane J. W. (1994). *J. Appl. Phys.*, 76, 1331.
- [5] Kent Displays Inc., Kent, OH44240, USA.
- [6] Merck Ltd. Merck House, Southampton, UK.
- [7] LeClere, D., Mughal, A., & Gleeson, H. F. (2002) MPhys Report, Department of Physics and Astronomy, University of Manchester.
- [8] Fergason, J. L. (1966). *Liq. Cryst. Proc. 2nd Kent conf.*
- [9] Berreman, D. (1972). *J. Opt. Soc. Am.*, 62, 502.
- [10] Gleeson, H. F. & Coles, H. (1989). *Mol. Cryst. Liq. Cryst.*, 170, 9.
- [11] E.g. Jenkins, F. A. & White, H. E. (1981). *Fundamentals of Optics*, 4th Edition, McGraw-Hill Book Company International Editions., Physics Series, Auckland.
- [12] Dreher, R., Meier, G., & Saupe, A. (1971). *Mol. Cryst. Liq. Cryst.*, 13, 17.
- [13] Muller, W. U. & Stegemeyer, H. (1973). *Ber. Buns.*, 77, 20.
- [14] Guillou, J.-P. (2001). MSc Thesis, Department of Physics and Astronomy, Manchester University.
- [15] Chen, S. H., Katsis, D., Schmid, A. W., Mastrangelo, J. C., Tsutsui, T., & Blanton, T. N. (1999). *Nature*, 397(6719), 506.
- [16] Azzum, R. M. A. & Bashara, N. M. (1996). *Ellipsometry and Polarized Light*, Elsevier Science B.V.: Amsterdam.